

# Direct Observation on the Evolution of Shear Banding and Buckling in Tungsten Fiber Reinforced Zr-Based Bulk Metallic Glass Composite

J.H. CHEN, Y. CHEN, M.Q. JIANG, X.W. CHEN, H.M. FU, H.F. ZHANG, and L.H. DAI

The evolution of micro-damage and deformation of each phase in the composite plays a pivotal role in the clarification of deformation mechanism of composite. However, limited model and mechanical experiments were conducted to reveal the evolution of the deformation of the two phases in the tungsten fiber reinforced Zr-based bulk metallic glass composite. In this study, quasi-static compressive tests were performed on this composite. For the first time, the evolution of micro-damage and deformation of the two phases in this composite, *i.e.*, shear banding of the metallic glass matrix and buckling deformation of the tungsten fiber, were investigated systematically by controlling the loading process at different degrees of deformation. It is found that under uniaxial compression, buckling of the tungsten fiber occurs first, while the metallic glass matrix deforms homogeneously. Upon further loading, shear bands initiate from the fiber/matrix interface and propagate in the metallic glass matrix. Finally, the composite fractures in a mixed mode, with splitting in the tungsten fiber, along with shear fracture in the metallic glass matrix. Through the analysis on the stress state in the composite and resistance to shear banding of the two phases during compressive deformation, the possible deformation mechanism of the composite is unveiled. The deformation map of the composite, which covers from elastic deformation to final fracture, is obtained as well.

DOI: 10.1007/s11661-014-2493-9

© The Minerals, Metals & Materials Society and ASM International 2014

## I. INTRODUCTION

DUE to the unique microstructure, bulk metallic glasses (BMGs) have a series of excellent mechanical and physical properties.<sup>[1–6]</sup> They have shown widespread potential applications in many fields.<sup>[7–10]</sup> However, plastic deformation of BMGs at room temperature is prone to be highly localized into nanoscale shear bands.<sup>[11–14]</sup> The easy nucleation and rapid propagation of shear bands can induce catastrophic fracture with very limited ductility,<sup>[15–20]</sup> impeding the further applications of BMGs. The fabrication of BMG matrix composites with ductile crystalline metal as reinforcement materials has yielded improvements in mechanical behavior<sup>[21–28]</sup>; *e.g.*, the *in situ* dendrite/BMG matrix composites exhibit increased both tensile and compressive

strains to failure.<sup>[22–28]</sup> Previous studies<sup>[22–24]</sup> have pointed out that the ductile crystalline phase in the BMG matrix composite may have a dual role in the response of mechanical loading; they may serve as heterogeneous sites for the initiation of individual shear bands, while at the same time act as attraction or pinning centers during shear band propagation. Both aspects facilitate the generation of multiple shear bands which can accommodate much plastic strain. Due to these multiple shear bands, the macroscopic plasticity of the BMG can be improved to a great extent.

Since it was first fabricated by Dandliker *et al.*,<sup>[29]</sup> the tungsten fiber reinforced Zr-based BMG matrix composite has attracted much attention in the past few years.<sup>[30–42]</sup> This composite has considerable plasticity under both quasi-static and dynamic compression.<sup>[30,32–38,40]</sup> In addition, due to its self-sharpening behavior under high speed impact, this composite penetrator has approximately a 10 to 20 pct improvement in penetration efficiency over the traditional tungsten heavy alloys.<sup>[31]</sup> This unique property promotes the tungsten fiber reinforced Zr-based BMG matrix composite to be applied effectively to defense industry.<sup>[31,41]</sup>

Many previous studies had focused on the macroscopic properties of this composite.<sup>[30–42]</sup> Conner *et al.*<sup>[30]</sup> studied the quasi-static tensile and compressive properties of tungsten fiber reinforced  $Zr_{41.25}Ti_{13.75}Cu_{12.5}Ni_{10}Be_{22.5}$  metallic glass matrix composite. It was found that the compressive failure mode for this composite changes from the shear banding to localized fiber buckling and tilting as fiber volume fraction

---

J.H. CHEN, Ph.D. Candidate, and Y. CHEN and M.Q. JIANG, Associate Professors, are with the State Key Laboratory of Nonlinear Mechanics, Institute of Mechanics, Chinese Academy of Sciences, Beijing 100190, P.R. China. X.W. CHEN, Professor, is with Institute of Systems Engineering, China Academy of Engineering Physics, Mianyang, Sichuan 621999, P.R. China. H.M. FU, Associate Professor, and H.F. ZHANG, Professor, are with Shenyang National Laboratory for Materials Science, Institute of Metal Research, Chinese Academy of Sciences, Shenyang 110016, P.R. China. L.H. DAI, Professor, is with the State Key Laboratory of Nonlinear Mechanics, Institute of Mechanics, Chinese Academy of Sciences, and also with State Key Laboratory of Explosion Science and Technology, Beijing Institute of Technology, Beijing 100081, P.R. China. Contact e-mail: lhdai@lnm.imech.ac.cn

Manuscript submitted May 5, 2014.

Article published online August 7, 2014

increases. Qiu *et al.*<sup>[32]</sup> conducted compressive experiments on the tungsten fiber reinforced ZrAlNiCuSi BMG matrix composite. Their results are consistent with the observations of Conner *et al.* Subsequently, Zhang *et al.*<sup>[34]</sup> proposed that the failure mode of this composite at room temperature is decided by the critical stress for shear fracture and splitting fracture. Lee *et al.*<sup>[39]</sup> directly observed the micro-fracture processes of the Zr-based BMG matrix composites reinforced with continuous metallic fibers. They suggested that the fracture properties of BMG matrix composites reinforced with metallic continuous fibers are heavily influenced by the properties of reinforcing fibers. From these studies, it can be concluded that the properties of the tungsten fiber reinforced BMG matrix composite are strongly affected by the microstructure. However, the correlation between the microstructure and properties of this composite is unknown, *i.e.*, the deformation mechanism still remains elusive.

Actually, the crystalline tungsten fiber and amorphous matrix have intrinsically different microstructures and deformation mechanisms. Under the external loading, the slender tungsten fiber is easy to lose its stability, resulting in buckling deformation.<sup>[30,32,33,35]</sup> However, shear bands are prone to nucleate and propagate in the BMG matrix due to its unique microstructure.<sup>[15–20]</sup> Tungsten fiber reinforced BMG matrix composite contains both these two phases. The interaction between these two different deformation mechanisms should affect the macroscopic properties of this composite, which deserves a further investigation.

In the present study, quasi-static compression was carried out on the tungsten fiber reinforced Zr-based BMG composite with 60 pct fiber volume fraction. In order to investigate the evolution of the micro-damage, the deformation process was “frozen” at five loading stages. At each deformation stage, the deformation and damage evolution of the tungsten fiber and BMG matrix were carefully examined. The deformation map of the composite, which covers from elastic deformation to final fracture, is obtained. The deformation mechanisms are discussed as well. Our results assist in more comprehensively understanding the evolution mechanism of the deformation and fracture, and in guiding microstructure design to enhance the plasticity of BMG composite.

## II. EXPERIMENTS

Zr<sub>41.2</sub>Ti<sub>13.8</sub>Ni<sub>12.5</sub>Cu<sub>10</sub>Be<sub>22.5</sub> (Vit 1) is chosen as the matrix. This BMG has excellent glass forming ability. Tungsten fiber with diameter of 300  $\mu\text{m}$  is selected as the reinforcement. The tungsten fiber/BMG matrix composite is prepared using infiltration and rapid solidification method. Details of the casting can be found elsewhere.<sup>[29]</sup> According to the previous studies,<sup>[30,32]</sup> the tungsten fiber/BMG matrix composite with a middle fiber volume fraction fractures in a mixed mode which combines shear banding and buckling. Understanding this complicated deformation mode may shed deep insight into the deformation mechanism of the BMG

composites. Thus, the composite with 60 pct fiber volume fraction is chosen as our experimental material. Figure 1(a) shows the XRD pattern of this composite. It can be seen that only the peaks of crystalline tungsten can be found. No other crystalline phases are detected within the sensitivity limit of the XRD. Microstructure of this composite is shown in Figure 1(b). The tungsten fibers are homogeneously distributed within the continuous glass matrix.

Quasi-static compressive specimens, which are 5 mm in diameter and 8 mm in length, are obtained by wire electrical discharge machining the as-cast composite rods using coolant. The specimen end surfaces are polished to be parallel to each other and perpendicular to the loading axis. The loading process comprises two steps: first the specimens are loaded to a certain level of plastic strain, and then they will be unloaded. To better understand the deformation process of the composite, a high speed camera, with a maximum framing rate capability of 300 thousand frames per second is used to image the deformation process. After testing, the optical microscope is used to characterize the macro-

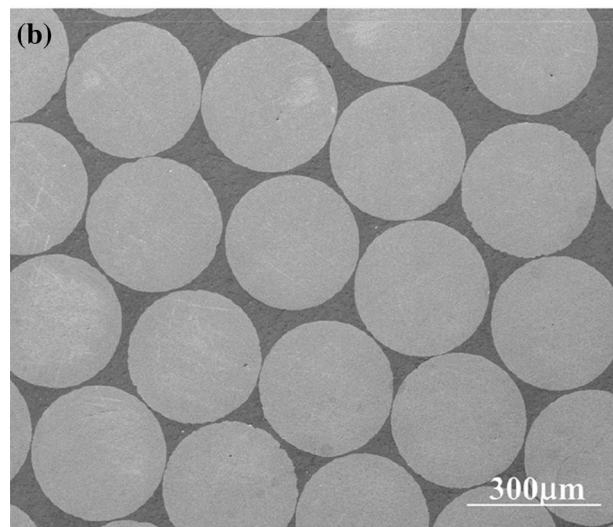
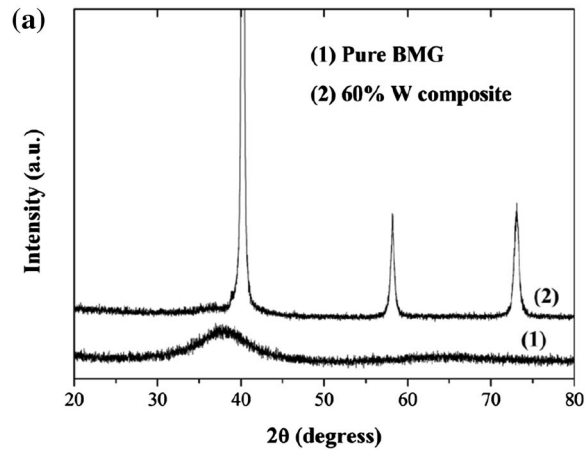


Fig. 1—(a) XRD pattern of the tungsten fiber/Vit1 BMG composite. (b) Microstructure of the tungsten fiber/Vit1 BMG composite.

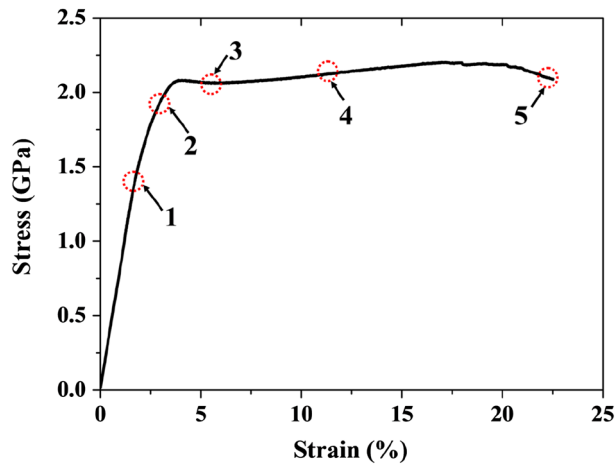


Fig. 2—Entire compressive stress–strain curve of the composite. Five different levels of deformation are indicated by the arrows.

scopic deformation of the specimen first, followed by scanning electron microscope (SEM) observation on the microscopic deformation. Furthermore, the buckling deformation of the tungsten fiber is carefully characterized by topologically scanning along the surface of the specimen using a 3D laser scanning confocal microscopy.

### III. RESULTS

Figure 2 shows the entire compressive stress–strain curve of the composite with 60 pct tungsten fiber volume fraction. In this study, deformation of the composite is frozen by loading–unloading at five different levels of macroscopic strain, as shown by the arrows in Figure 2. The detailed results of each deformation stage are shown in the following paragraphs.

Deformation morphologies of the specimen loaded to 1.7 pct strain are shown in Figure 3. Figure 3(a) shows the lateral surface of the specimen observed under the optical microscope. Details corresponding to the areas (1) to (3) marked in Figure 3(a) are shown in Figures 3(b) through (d), respectively. No shear bands can be found in the BMG matrix throughout the specimen, indicating that elastic or uniform plastic deformation occurs in it. In order to precisely characterize the deformation of the tungsten fiber, topological scan is taken along the red line marked in Figure 3(a), which is shown in Figure 3(e). Due to some polishing flaws remained in the matrix and traces left during the experiments, small peaks can be found in Figure 3(e). Once buckling deformation of the tungsten fiber occurs, the composite becomes thick in the middle. This makes the height in the middle part of the specimen becomes higher than the two ends. It can be seen from Figure 3(e) that the middle part is about  $5 \mu\text{m}$  higher than the ends of the specimen, indicating that micro-buckling occurs for the tungsten fiber.

Figure 4 shows the deformation morphologies of the specimen loaded to 2.7 pct strain. Details of the end of the specimen (area marked by (1) in (a)) are shown in

Figure 4(b). Shear bands can be observed in the BMG matrix, as shown by the arrows in this figure. Figure 4(c) is a magnified SEM picture of the shear bands. These shear bands are parallel to each other with a inclination angle of about 45 deg to the loading direction. Details corresponding to the area marked by (2) in Figure 4(a) are shown in Figure 4(d). However, no shear bands can be found in the middle part of the specimen. The early occurrence of shear bands at the end of the specimen may be caused by the stress concentration in these regions. Topological scan along the red line marked in Figure 4(a) is shown in Figure 4(e). The middle of specimen is nearly  $10 \mu\text{m}$  higher than the ends. Compared to the specimen with 1.7 pct strain, a heavier buckling deformation of the tungsten fiber occurs.

The lateral surface morphologies of composite with 5.0 pct strain are given in Figure 5. Profuse shear bands, indicated by the arrows in Figures 5(b) and (c), are observed in the middle part of the specimen. It can be seen from Figure 5(b) that the shear bands propagated from two edge sides meet together in the middle of the matrix. These shear bands interact with each other, inducing the branching of shear bands. These promote the generation of more shear bands in the matrix, which can accommodate more plastic strain and contribute to the macroscopic plasticity of the composite. However, these shear bands are constrained in the BMG matrix. No shear bands can be seen in the tungsten fiber. These indicate that shear bands initiate in the BMG matrix first. After initiation, shear bands will propagate in the matrix and can be hindered by the tungsten fibers when encountering them. Heavier buckling of the tungsten fiber is observed in this deformation stage, for the height of the middle part is much higher than the ends of the specimen, as shown by the topological scan in Figure 5(d).

For specimens with large deformation, a high speed camera is used to record the deformation process. Figure 6 gives the stress–strain curve and macroscopic deformation process of the composite with 12.6 pct strain. Buckling of the tungsten fiber can be seen obviously at large strain, as shown in Figure 6(d). Deformation morphologies of the tungsten fiber and BMG matrix are shown in Figure 7. Figure 7(c) gives details corresponding to the area marked in (b). It can be seen from this figure that in this deformation stage, the shear bands in the BMG matrix evolve into the shear cracks. Furthermore, these shear cracks induce shear deformation in the tungsten fiber. However, this shear deformation only occurs at the edge of the tungsten fiber. It cannot cross through the entire fiber.

Figure 8 shows the deformation process of the composite which is loaded to 23.0 pct strain. At this strain, the composite begins to lose its load capability, showing a softening behavior. Buckling deformation of the tungsten can be obviously observed at the 15.9 pct strain, as shown in Figure 8(c). The lateral surface morphologies of the fractured specimen are shown in Figure 9. Figures 9(b) through (d) are magnified images corresponding to the areas marked by (1) to (3) in Figure 9(a), respectively. In some local regions of the specimen, shear bands are still constrained in the BMG matrix, as can be seen from Figure 9(b). Figures 9(c)



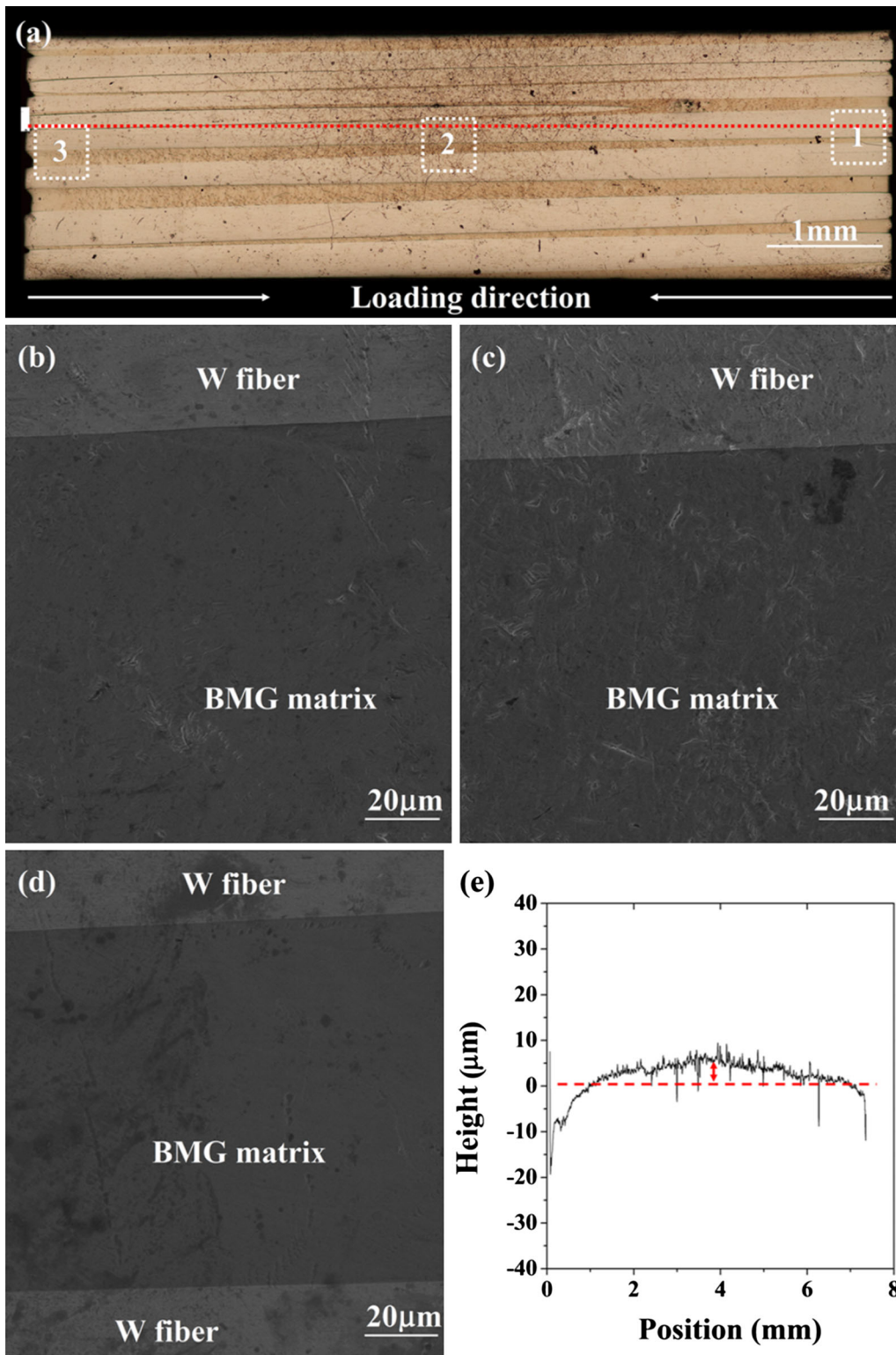


Fig. 3—Deformation morphologies of the composite in the first deformation stage. (a) Lateral morphologies observed under optical microscope. (b) through (d) Magnified images corresponding to the areas (1) to (3) marked in (a), respectively. (e) Topological scan along the red line marked in (a) (Color figure online).

and (d) show the cracks in the composite. It can be seen from these figures that the fibrous tungsten fiber attaches to the BMG matrix at the splitting crack. This

indicates that splitting occurs in the tungsten fiber near the fiber/matrix interface region. Simultaneously, shear fracture occurs in the BMG matrix.

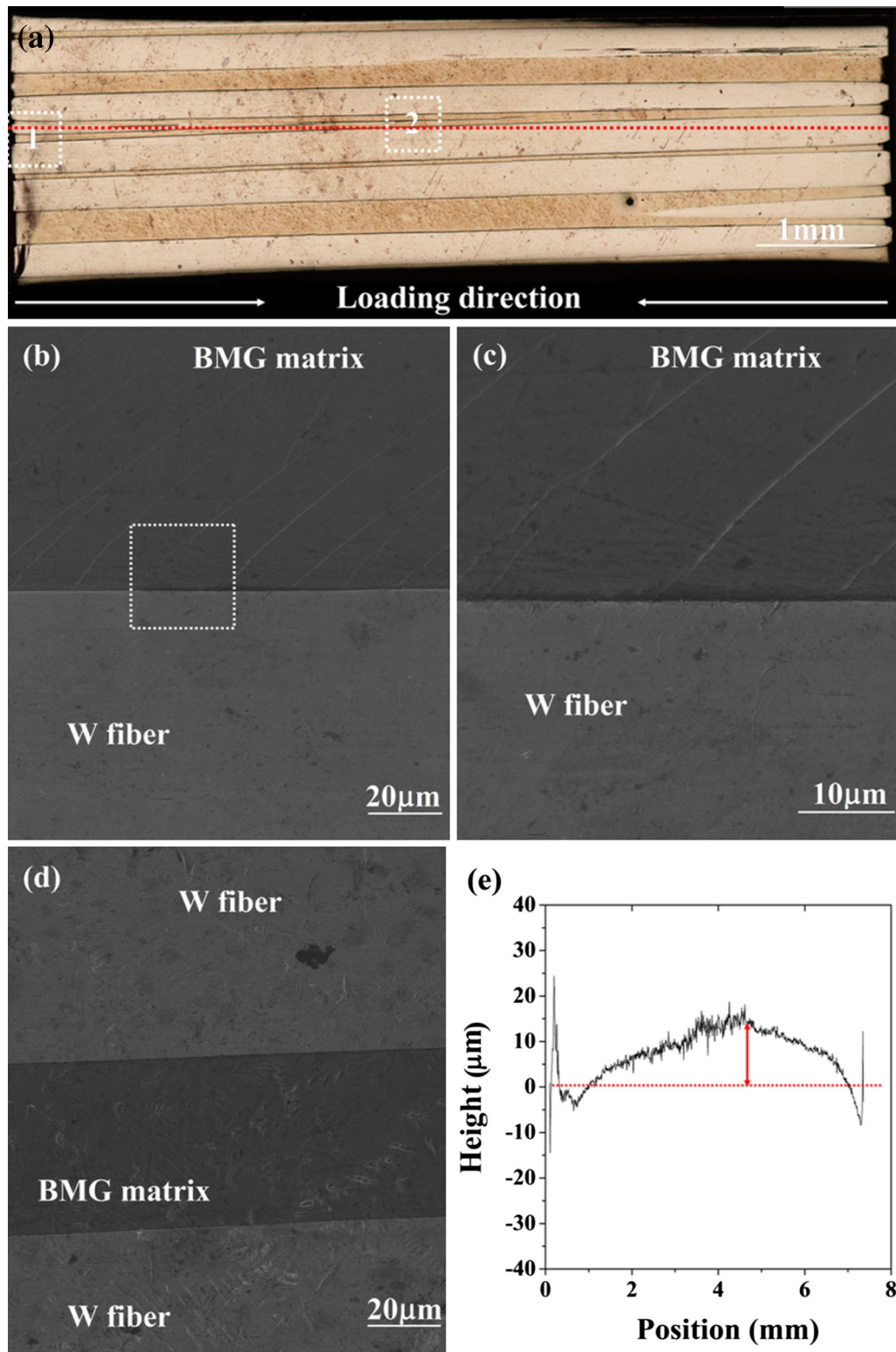


Fig. 4—Deformation morphologies of the composite in the second deformation stage. (a) Lateral morphologies of the composite. (b), (c) Shear bands in the area marked by (1) in (a). (d) Details of the area marked by (2) in (a). (e) Topological scan along the red line marked in (a) (Color figure online).

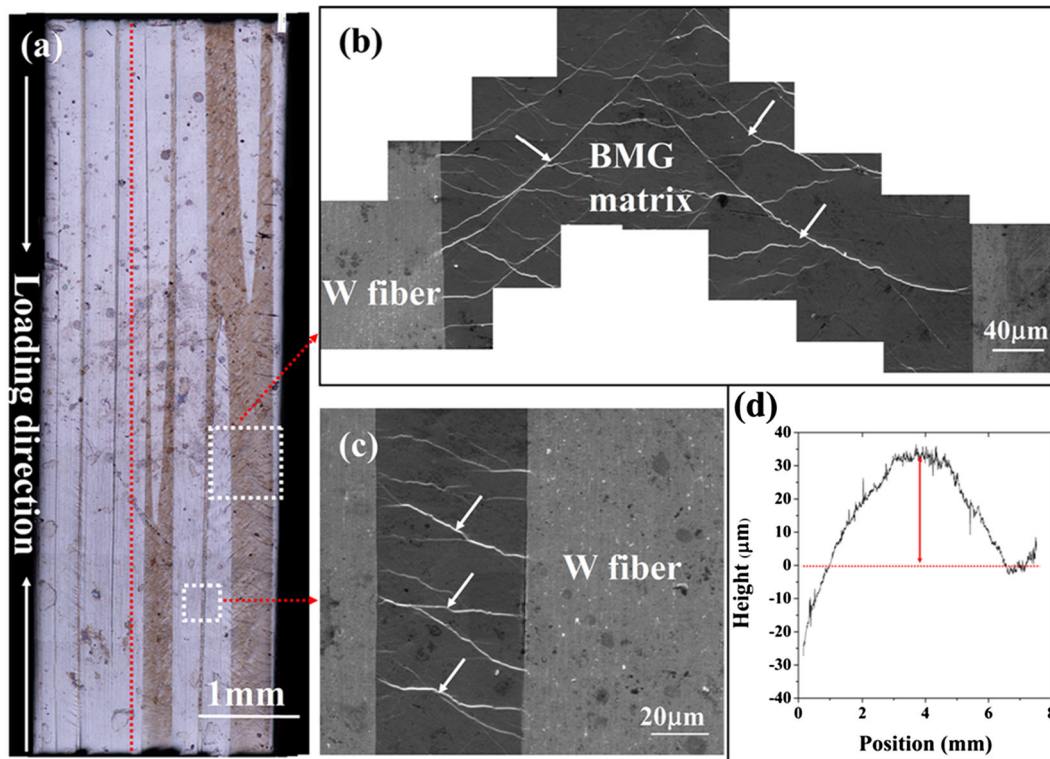


Fig. 5—Deformation morphologies of the composite in the third deformation stage. (a) Lateral morphologies of the composite. (b), (c) Shear bands in the lateral surface of the specimen. (d) Topological scan along the red line marked in (a).

## IV. DISCUSSION

### A. Information Extracted from Experiments

The experimental results and observations uncover some crucial features of tungsten fiber/BMG matrix composite behavior during deformation, as follows:

- (1) Upon the external loading, tungsten fiber in the composite is easy to lose its stability, resulting in buckling deformation. In the present experiments, buckling deformation of the tungsten fiber is observed at a small strain (1.7 pct), while the BMG matrix deforms homogeneously. The early buckling of the tungsten fiber may change the local stress state of the composite, which further affects the deformation of the composite. The mechanism for these will be discussed in the next section.
- (2) Shear bands in the composite initiate and propagate in the BMG matrix. When encountering the tungsten fiber, they will be hindered by the tungsten fiber or only cause the shear deformation at the edge of the tungsten fiber. These shear bands can hardly cross through the entire fiber. These indicate that the tungsten fiber has a stronger resistance to propagation of shear bands than the BMG matrix.
- (3) The occurrence of splitting fracture in the composite may be caused by transverse tensile stress, which deserves further investigation. Furthermore, splitting fracture happens within the tungsten fiber

near the fiber/matrix interface region, indicating that the tungsten fiber may have a weak transverse tensile strength.

### B. Deformation Mechanism

Based on the information got from the experiments, deformation mechanism of the composite is discussed in this section.

#### 1. Buckling of tungsten fiber

Under the external loading, the composite will behave elastically first. The composite contains the tungsten fiber and BMG matrix, the basic physical and mechanical properties of these two phases are listed in Table I.<sup>[30,43]</sup> Due to the mismatch of the elastic and thermal properties of these two phases, the load carried by the tungsten fiber is different from which carried by the BMG matrix. This load distribution will decide which phase will behave inelastically first. Two kinds of stress contribute to the stress distribution in the composite. One is the residual thermal stress. Upon cooling, unequal coefficients of the thermal expansion of the matrix and reinforcement cause thermal stress. The other is the stress caused by external load. Using the coaxial cylinder model proposed by Warwick and Clyne,<sup>[44]</sup> the matrix and fiber stress distribution for the composite with 60 pct fiber volume fraction can be calculated. In the first deformation stage in the present



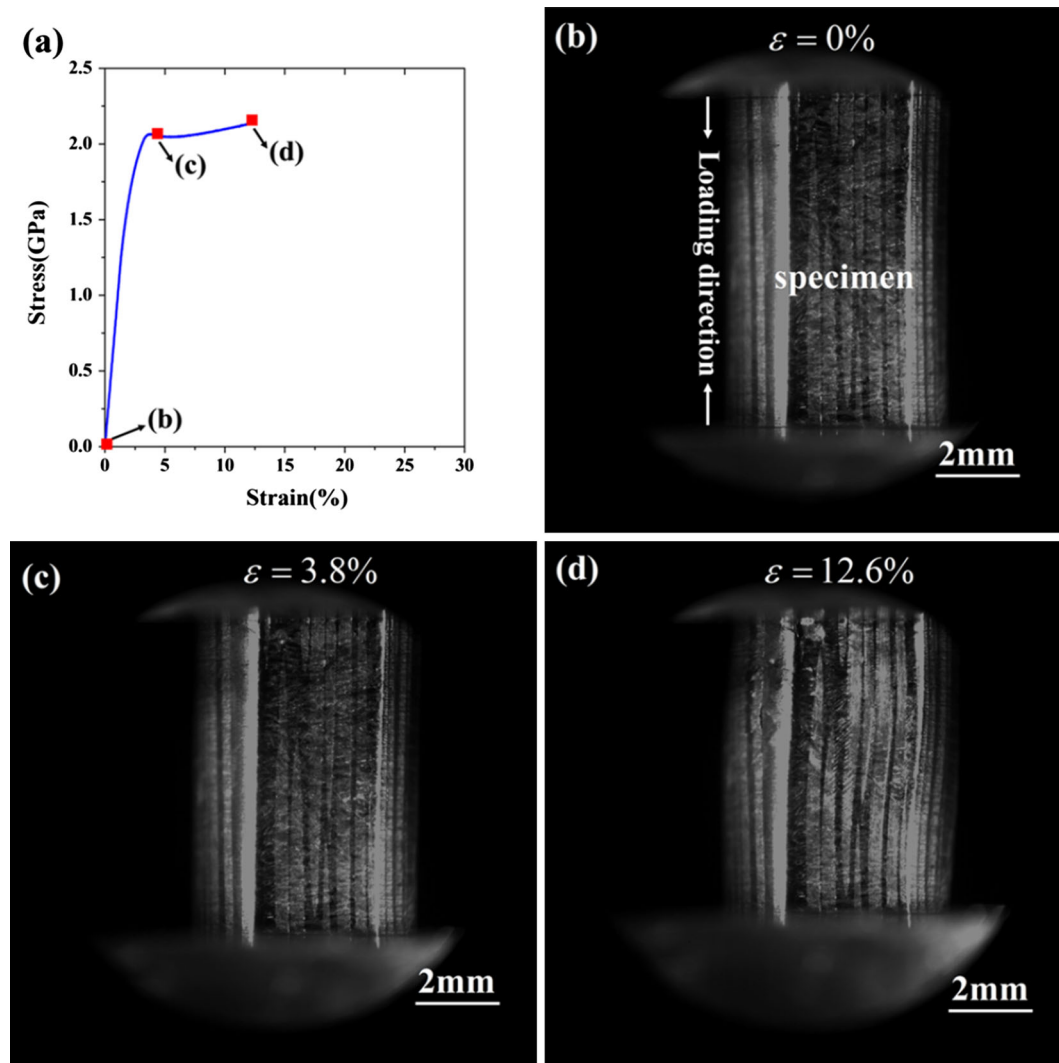


Fig. 6—(a) Stress–strain curve of the composite in the fourth deformation stage. (b) through (d) Macrographs of the specimen at different strains.

study, the composite has a strain of 1.7 pct, which corresponding to the stress of 1.4 GPa. Figure 10 is a graph of the calculated stresses in a 60 pct tungsten fiber volume fraction/Vit1 BMG composite which combines the residual thermal stress and a 1.4 GPa axial load. From this figure, it can be seen that under this load, the stress withstood by the tungsten fiber is as high as about 2.1 GPa. However, axial stress in the BMG matrix is only 0.4 GPa.

According to the conventional Euler buckling model,<sup>[45]</sup> the critical stress,  $\sigma_{cr}$ , for a slender bar of a length  $l$  (Figure 11(a)), is

$$\sigma_{cr} = \frac{\pi^2 E}{(\mu l/i)^2}, \quad [1]$$

where  $E$  is the Young's modulus,  $i$  is the smallest radius of inertia of the cross section, and  $\mu$  is a dimensionless factor depending on the end restraints. For the present tungsten fiber/Vit1 BMG composite, diameter and

length of the tungsten fiber are  $300 \mu\text{m}$  and  $8.0 \text{ mm}$ , respectively. Young's modulus is given in Table I. Substituting the values of parameters into Eq. [1] and  $\sigma_{cr} = 0.36 \text{ GPa}$  is obtained. This indicates that if no lateral support exists, the critical stress, for the tungsten fiber to lose its stability, is only 0.36 GPa. However, the tungsten fiber is surrounded by the BMG matrix, which acts as the lateral support to the fiber. This will prevent the instability of the fiber. For the extreme condition, the surrounded BMG is infinite, as shown in Figure 11(b). The critical stress  $\sigma_{cr}$  for the tungsten fiber is the yield strength, which is 1.4 GPa.<sup>[43]</sup> Actually, for the composite with 60 pct fiber volume fraction in the present study, only finite lateral support to the tungsten fiber can be provided by the matrix. Thus, the critical stress of the tungsten fiber will lie between 0.36 and 1.4 GPa, *i.e.*,  $0.36 \text{ GPa} < \sigma_{cr} < 1.4 \text{ GPa}$ .

From Figure 10, the stress withstood by the tungsten fiber is about 2.1 GPa when the external load is 1.4 GPa. This stress is higher than the critical stress

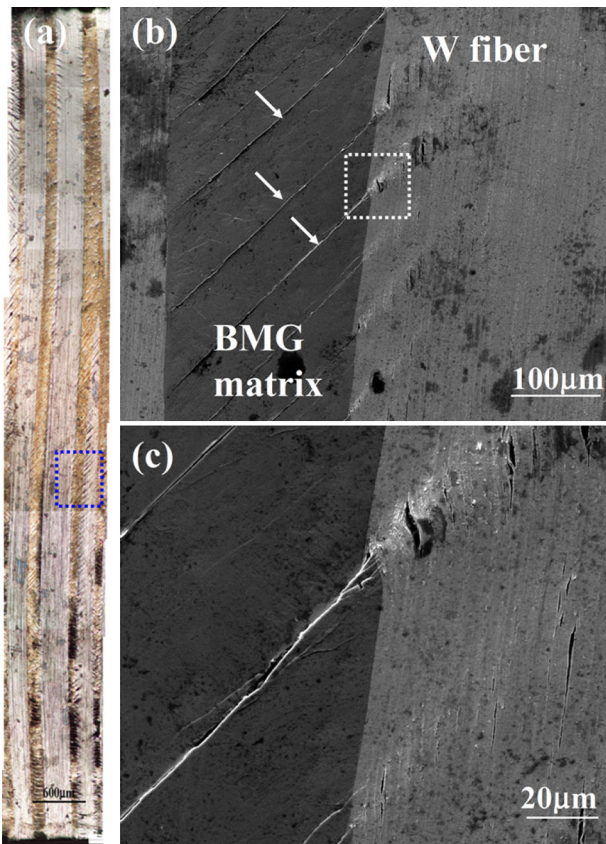


Fig. 7—Lateral surface of the specimen in the fourth deformation stage. (a) through (c) Deformation morphologies of the composite at different magnifications.

$\sigma_{cr}$  of the tungsten fiber, indicating that the buckling deformation occurs. However, the axial and hoop stress of the matrix are 250 MPa in compression and 250 MPa in tension, respectively. It is assumed that yielding (in tension or compression) begins when the Von Mises stress on the BMG matrix reaches the matrix yield strength. The Mises stress of the matrix is calculated, which has the value of 433 MPa. This is much lower than the matrix yield strength (1.8 GPa<sup>[46–48]</sup>). Thus, it can be concluded that when the tungsten fiber begins to buckle, the BMG matrix still deforms elastically.

From Table I, it can be seen that the Young's modulus of the tungsten fiber is about four times higher than the BMG matrix. Due to its high Young's modulus, the stress carried by the tungsten fiber is much higher than the stress sustained by the BMG matrix. This high stress, combined with the slender structure of tungsten fiber, resulting in the early buckling deformation of the tungsten fiber. Because of the low stress sustained by it and its high yield strength, the BMG matrix behaves elastically when buckling of the tungsten fiber occurs.

## 2. Initiation and propagation of shear bands

Upon further loading, the tungsten fiber continues buckling (Figures 4(e) and 5(d)). Once the elastic deformation of BMG matrix cannot accommodate further deformation any more, shear bands will initiate in the BMG matrix. Profuse shear bands, which initiate from the

fiber/matrix interface and propagate toward the center of the matrix, are observed in the third deformation stage in the present experiments (Figure 5(b)). These shear band patterns are similar to the shear bands observed on the BMG beam which subjects to bending load.<sup>[49,50]</sup> Actually, buckling of the tungsten fiber will change the local stress state in the composite, which makes the stress state deviate from the uniaxial stress state. Bending deformation will occur for the BMG matrix, as shown in Figures 6(d) and 7(a). Under bending, the fiber/matrix interfaces will act as the nucleation sites for the shear bands, for higher stress exists in these regions.<sup>[49–51]</sup>

In the present composite with 60 pct fiber volume fraction, when the shear bands encounter the tungsten fiber, they can hardly induce shear deformation of the tungsten fiber (Figure 5(c)). In the fourth deformation stage in the present experiments, shear bands in the BMG matrix evolve into shear cracks. These shear cracks induce shear deformation at the edge of the tungsten fiber (Figure 7(c)). However, these shear bands in the tungsten fiber can hardly cross through the entire tungsten fiber (Figure 7(b)). It can be seen from these that the tungsten fiber acts as the obstacle for the propagation of shear bands.

In the previous studies,<sup>[52–54]</sup> shear band toughness, which reflects the critical plastic energy dissipated in the shear band, is proposed to measure the intrinsic resistance of materials to propagation of shear bands. Larger shear band toughness indicates more significant resistance of materials to the propagation of the shear bands. The crystalline tungsten and amorphous matrix have different energy dissipation mechanisms of shear band. In addition to conventional thermal/energy and momentum/viscous dissipation in the crystalline tungsten, the free volume dissipation should be involved in the BMG matrix due to its unique structure. The shear band toughness of the tungsten was calculated by Grady,<sup>[53]</sup> which has the value of  $138.5 \text{ MPa}\sqrt{\text{m}}$ . In our previous work,<sup>[54]</sup> the concept of shear band toughness was developed in the amorphous alloys. The shear band toughness of 2.7 to  $26.6 \text{ MPa}\sqrt{\text{m}}$  is obtained for the Vit1 BMG. It can be seen that the shear band toughness of the tungsten is 1 to 2 order of magnitude higher than that of the BMG matrix. This indicates that the tungsten fiber has a stronger resistance to propagation of shear band than the matrix. Thus, when the shear bands encounter the tungsten fiber, they will be hindered by the tungsten fiber. The tungsten fiber acts as the obstacle for the propagation of shear bands.

## 3. Splitting of the composite

In the later deformation stage of the composite, *i.e.*, the fourth and fifth deformation stage in the present experiments, buckling of the tungsten fiber can be seen obviously from the macrographs imaged by the high speed camera (Figures 6(d) and 8(c)). Further buckling of the tungsten fiber will result in splitting fracture in the composite (Figure 8(d)). As mentioned in the above section, buckling of the tungsten fiber will change the local stress state in the composite, which makes the stress state deviate from the uniaxial stress state. Bending deformation will occur for the tungsten fiber. This can be seen from Figures 6(d) and 7(a). Under



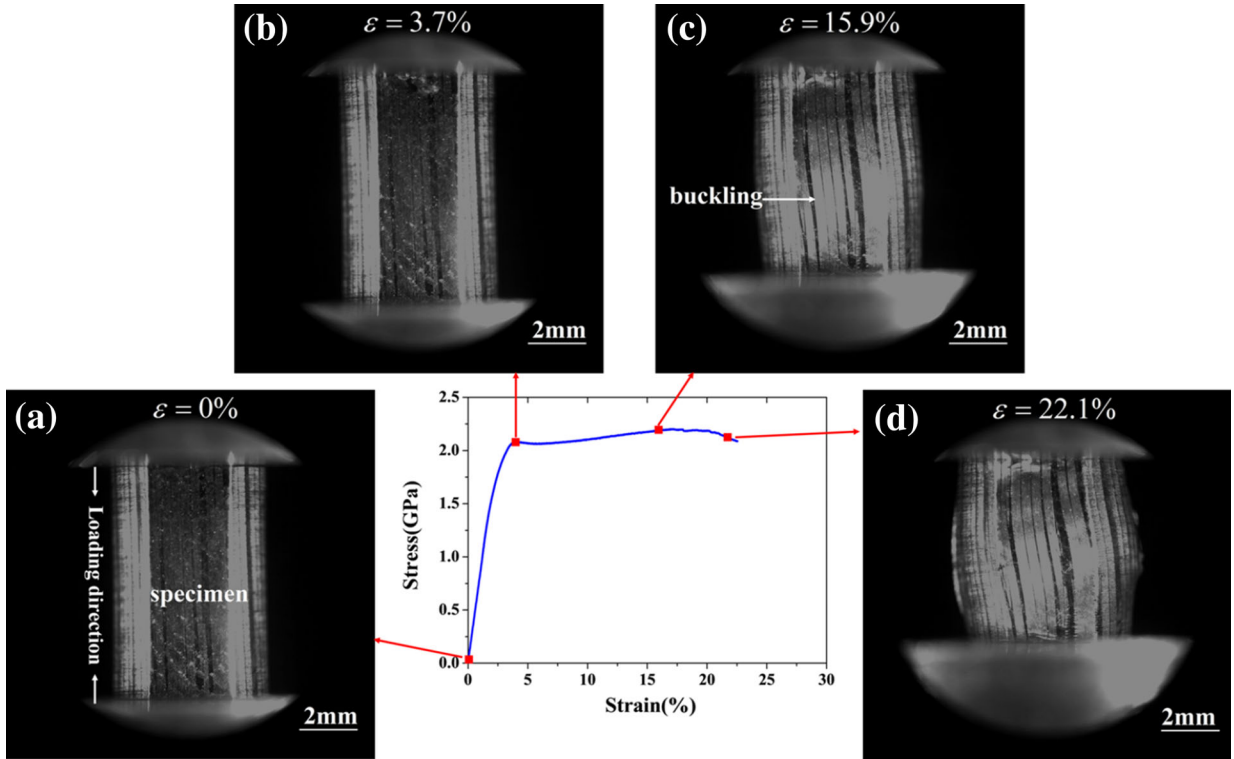


Fig. 8—Deformation process of the composite in the fifth deformation stage.

bending, higher stress exists at the boundary of the fiber quite close to the fiber/matrix interface. Thus, splitting fracture is easier to occur near the interface rather than the middle of the tungsten fiber. Schematic illustration of buckling deformation of the tungsten fiber is shown in Figure 12. Supposing the deflection of the tungsten fiber can be expressed by

$$u_x = a_1 \sin \frac{\pi x}{l}. \quad [2]$$

The coordinate axes are shown in Figure 12(b).  $u_x$  is the deflection of the tungsten fiber at position  $x$ ,  $a_1$  is the maximum deflection which locates in the middle of the tungsten fiber,  $l$  is the length of the tungsten fiber.

Deflection of tungsten fiber will cause transverse tensile strain of the composite, which can be given by

$$\varepsilon_x = \frac{2u_x}{a} = \frac{2a_1}{a} \sin \frac{\pi x}{l}, \quad [3]$$

where  $a$  is the width of the specimen. Supposing this transverse tensile strain distributes homogeneously along the width of the specimen, and the BMG matrix and tungsten fiber behave elastically. Then the transverse tensile stress in the matrix and tungsten fiber can be given by

$$\sigma_m = E_m \varepsilon_x, \quad [4]$$

$$\sigma_f = E_f \varepsilon_x, \quad [5]$$

respectively.

The tensile strength of Vit1 BMG is 1.8 GPa, while the Young's modulus is 96 GPa.<sup>[46–48]</sup> From Eq. [4], the critical tensile strain of 1.87 pct is obtained for the Vit1 BMG. The as-drawn tungsten fiber is used as the reinforcement in the composite in the present study. This tungsten fiber has fibrous grain boundary along the longitudinal fiber direction.<sup>[34,55]</sup> It has been estimated that the lateral grain boundary strength of a tungsten fiber with fibrous grain structure is only about 14 pct of its axial tensile strength.<sup>[56]</sup> Hence it can be proposed that the transverse tensile strength of the tungsten fiber is only about 300 MPa, since the axial strength is as high as 2.35 GPa.<sup>[30]</sup> The critical transverse tensile strain can be obtained from Eq. [5], which has the value of 0.07 pct. It can be seen that the critical tensile strain of the tungsten fiber is much lower than that of the BMG matrix. Thus, splitting fracture occurs preferentially in the tungsten fiber.

At the later deformation stage of the composite, splitting fracture occurs in the tungsten fiber due to lateral tensile stress and low lateral strength. At the same time, shear bands evolve into the shear cracks. Because of the strong resistance to the propagation of the shear deformation, shear banding and shear cracking can only occur in the BMG matrix. As a result, the composite fractures in a mixed mode, with shear fracture in the BMG matrix, along with splitting fracture in the tungsten fiber, as shown in Figure 9.

### C. Three Stages Deformation of the Composite

According to the aforementioned analysis of deformation mechanism of the tungsten fiber/Vit1 BMG

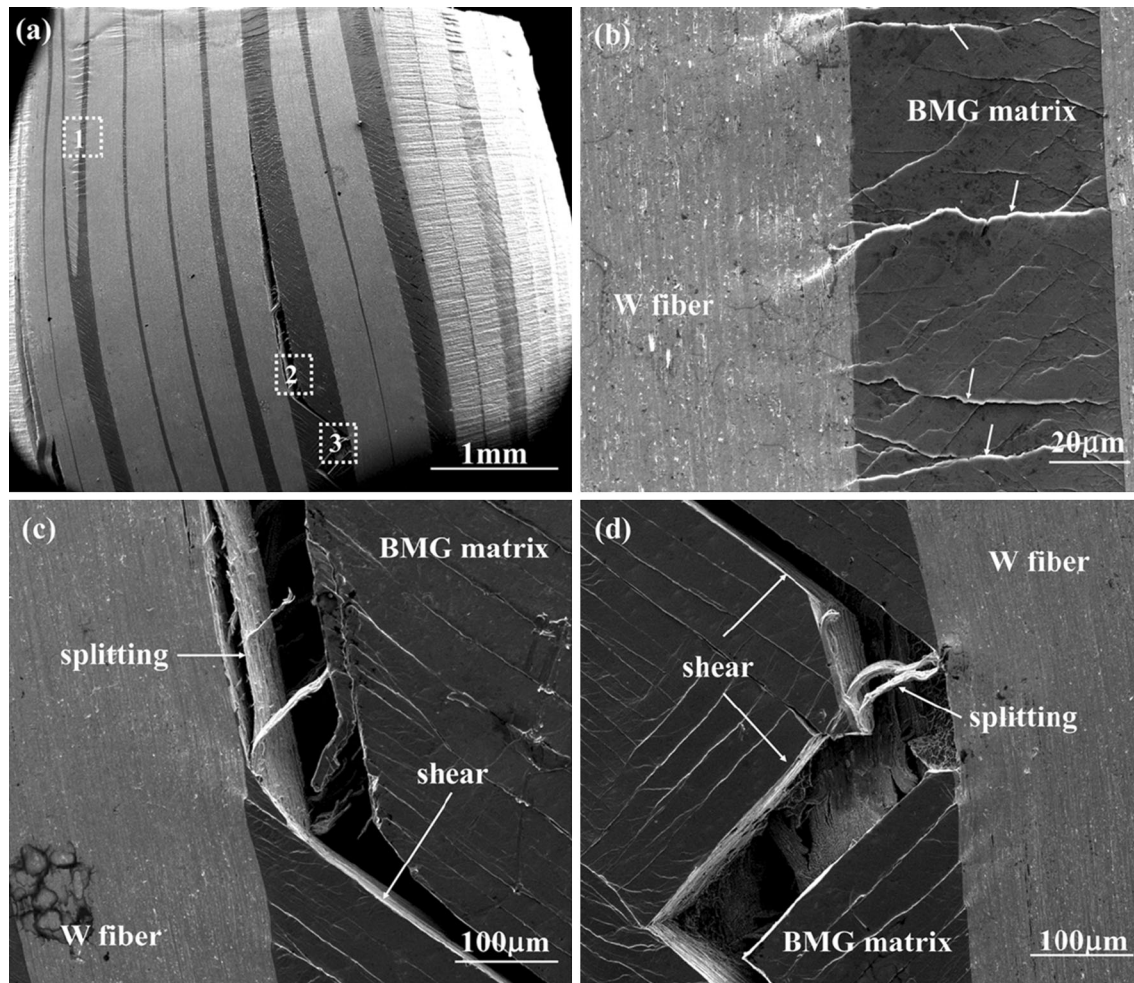


Fig. 9—(a) Lateral surface of the composite in the fifth deformation stage. (b) through (d) Details corresponding to the areas (1) to (3) marked in (a), respectively.

**Table I. Physical Properties of Vit1 BMG and Tungsten Fiber**

Properties	Vit 1 BMG	Tungsten Fiber
Young's modulus (GPa)	96	410
Shear modulus (Gpa)	34.3	160.5
Poisson's ratio	0.36	0.28
Thermal expansion coefficient ( $10^{-6}/^{\circ}\text{C}$ )	8.5	4.5
Compressive yield strength (GPa)	2.0	1.4

composite, the evolution of shear banding and buckling can be characterized by three stages. Details of each stage will be discussed in the following paragraphs.

In the first stage, due to its high stiffness, the tungsten fiber withstands a considerable amount of applied loads, which promotes early buckling of the tungsten fiber. The BMG matrix retains elastic deformation.

In the second stage, elastic deformation of the BMG matrix cannot accommodate further bending deformation any more. Shear bands initiate from the fiber/matrix interfaces for higher stresses exist in these

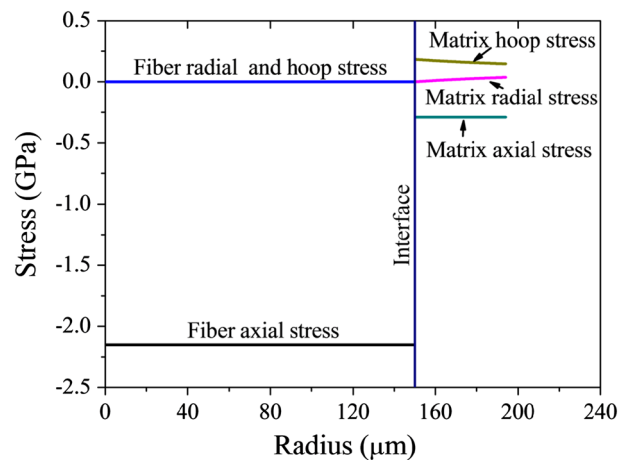


Fig. 10—Matrix and fiber stress distribution for the composite with 60 pct tungsten fiber volume fraction, including thermal residual stresses and 1400 MPa axial load.

regions. Shear bands propagate in the BMG matrix, when they encounter the tungsten fibers, they will be hindered by the tungsten fibers since the tungsten fibers

have strong resistance to the propagation of shear bands. On the one hand, shear bands can soften the strength of BMG.<sup>[57]</sup> On the other hand, shear banding in the matrix is hindered by the tungsten fiber, which increases the load capacity of the composite. Competition between these two aspects results in that the strength of the composite maintains constantly. Tungsten fibers continue buckling, resulting in transverse tensile stress in the composite.

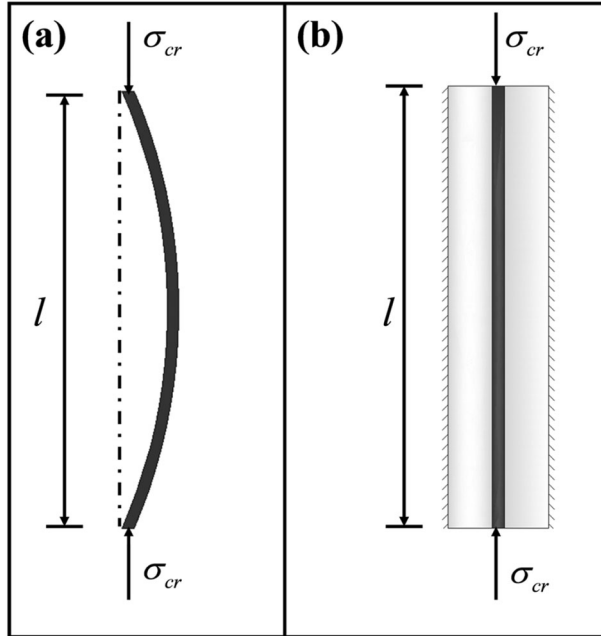


Fig. 11—(a) Buckled fiber without any lateral support. (b) Compressed fiber with solid lateral support.

In the third stage, the transverse tensile stress which is created by the buckled tungsten fiber overcomes the lateral tensile strength of the tungsten fiber, splitting fracture occurs in the tungsten fiber. Simultaneously, shear cracks propagate in the BMG matrix. These two aspects lead to the mixed failure mode for the composite.

## V. CONCLUSIONS

Quasi-static compressive experiments were conducted on the tungsten fiber reinforced  $Zr_{41.2}Ti_{13.8}Ni_{12.5}Cu_{10}Be_{22.5}$  BMG composite with 60 pct fiber volume fraction. The loading process was stopped at five different degrees of deformation in order to investigate the evolution of shear banding and buckling. Under external loading, buckling deformation occurs first, while the BMG matrix deforms elastically. This early buckling of the tungsten fiber is due to the considerable amount of applied load withstood by it. With further loading, shear bands initiate from the fiber/matrix interfaces for higher stress exists in these regions. Shear bands propagate in the BMG matrix, when they encounter the tungsten fiber, they will be hindered by the tungsten fiber for the tungsten fiber has strong resistance to the propagation of shear bands. Buckled tungsten fiber creates lateral tensile stress in the composite. Moreover, tungsten fiber has weak lateral tensile strength due to its fibrous microstructure along the longitudinal fiber direction. Splitting fracture is easy to occur in the tungsten fiber. Finally, the composite fractures in a mixed mode, with splitting in the tungsten fiber, along with shear fracture in the metallic glass matrix. According to the experimental results and

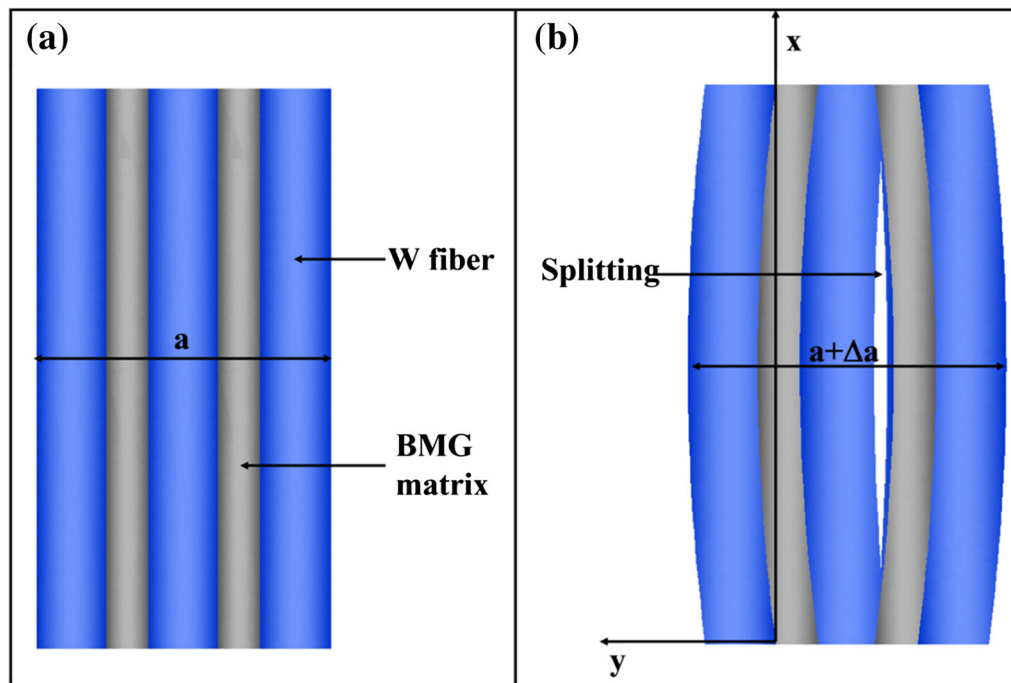


Fig. 12—Schematic illustration of buckling deformation of the tungsten fiber.



theoretical analysis, the three stages deformation is proposed to characterize the deformation mechanism of the composite.

## ACKNOWLEDGMENTS

Financial support is from the NSFC (Grants Nos. 11132011, 11202221, 11372315), the National Key Basic Research Program of China (Grant No. 2012CB937500). Research supported by the CAS/SA-IEA International Partnership Program for Creative Research Teams.

## REFERENCES

1. A.L. Greer: *Science*, 1995, vol. 267, pp. 1947–53.
2. W.H. Wang: *J. Appl. Phys.*, 2006, vol. 99, pp. 093506-1–093506-10.
3. C.A. Schuh, T.C. Hufnagel, and U. Ramamurty: *Acta Mater.*, 2007, vol. 55, pp. 4067–09.
4. J. Xu, U. Ramamurty, and E. Ma: *JOM*, 2010, vol. 62, pp. 10–18.
5. M.M. Trexler and N.N. Thadhani: *Prog. Mater. Sci.*, 2010, vol. 55, pp. 759–839.
6. W.H. Wang: *Prog. Mater. Sci.*, 2012, vol. 57, pp. 487–656.
7. M.F. Ashby and A.L. Greer: *Scripta Mater.*, 2006, vol. 54, pp. 321–26.
8. N. Nishiyama, K. Amiya, and A. Inoue: *J. Non-Cryst. Solids*, 2007, vol. 353, pp. 3615–21.
9. A. Inoue and A. Takeuchi: *Acta Mater.*, 2011, vol. 59, pp. 2243–67.
10. X. Huang, Z. Ling, Z.D. Liu, H.S. Zhang, and L.H. Dai: *Int. J. Impact Eng.*, 2012, vol. 42, pp. 1–10.
11. J. Li, F. Spaepen, and T.C. Hufnagel: *Philos. Mag. A*, 2002, vol. 82, pp. 2623–30.
12. X.F. Gu, K.J.T. Livi, and T.C. Hufnagel: *Mater. Res. Soc. Symp. Proc.*, 2003, vol. 754, pp. CC7.9.1–7.9.6.
13. Y. Zhang and A.L. Greer: *Appl. Phys. Lett.*, 2006, vol. 89, pp. 071907-1–071907-3.
14. M.Q. Jiang, W.H. Wang, and L.H. Dai: *Scripta Mater.*, 2009, vol. 60, pp. 1004–07.
15. W.J. Wright, T.C. Hufnagel, and W.D. Nix: *J. Appl. Phys.*, 2003, vol. 93, pp. 1432–37.
16. L.H. Dai, M. Yan, L.F. Liu, and Y.L. Bai: *Appl. Phys. Lett.*, 2005, vol. 87, pp. 14196-1–14196-3.
17. L.F. Liu, L.H. Dai, Y.L. Bai, and B.C. Wei: *J. Non-Cryst. Solids*, 2005, vol. 351, pp. 3259–70.
18. L.H. Dai and Y.L. Bai: *Int. J. Impact Eng.*, 2008, vol. 35, pp. 704–19.
19. M.Q. Jiang and L.H. Dai: *J. Mech. Phys. Solids*, 2009, vol. 57, pp. 1267–92.
20. A.L. Greer, Y.Q. Cheng, and E. Ma: *Mater. Sci. Eng. R*, 2013, vol. 74, pp. 71–132.
21. H.C.-Yim, R. Busch, U. Köster, and W.L. Johnson: *Acta Mater.*, 1999, vol. 47, pp. 2455–62.
22. C.C. Hays, C.P. Kim, and W.L. Johnson: *Phys. Rev. Lett.*, 2000, vol. 84, pp. 2901–04.
23. C.C. Hays, C.P. Kim, and W.L. Johnson: *Mater. Sci. Eng. A*, 2001, vols. 304–306, pp. 650–55.
24. D.C. Hofmann, J.-Y. Suh, A. Wiest, G. Duan, M.-L. Lind, M.D. Demetriou, and W.L. Johnson: *Nature*, 2008, vol. 451, pp. 1085–89.
25. Y. Wu, Y.H. Xiao, G.L. Chen, C.T. Liu, and Z.P. Lu: *Adv. Mater.*, 2010, vol. 22, pp. 2770–73.
26. J.W. Qiao, A.C. Sun, E.W. Wang, Y. Zhang, P.K. Liaw, and C.P. Chuang: *Acta Mater.*, 2011, vol. 59, pp. 4126–37.
27. Y. Wu, D.Q. Zhou, W.L. Song, H. Wang, Z.Y. Zhang, D. Ma, X.L. Wang, and Z.P. Lu: *Phys. Rev. Lett.*, 2012, vol. 109, pp. 245506-1–245506-5.
28. J.H. Chen, M.Q. Jiang, Y. Chen, and L.H. Dai: *Mater. Sci. Eng. A*, 2013, vol. 576, pp. 134–39.
29. R.B. Dandliker, R.D. Conner, and W.L. Johnson: *J. Mater. Res.*, 1998, vol. 13, pp. 2896–2901.
30. R.D. Conner, R.B. Dandliker, and W.L. Johnson: *Acta Mater.*, 1998, vol. 46, pp. 6089–6102.
31. R.D. Conner, R.B. Dandliker, V. Scruggs, and W.L. Johnson: *Int. J. Impact Eng.*, 2000, vol. 24, pp. 435–44.
32. K.Q. Qiu, A.M. Wang, H.F. Zhang, B.Z. Ding, and Z.Q. Hu: *Intermetallics*, 2002, vol. 10, pp. 1283–88.
33. G. Wang, D.M. Chen, J. Shen, Z.H. Stachurski, Q.H. Qin, J.F. Sun, and B.D. Zhou: *J. Non-Cryst. Solids*, 2006, vol. 352, pp. 3872–78.
34. H. Zhang, Z.F. Zhang, Z.G. Wang, K.Q. Qiu, H.F. Zhang, and Q.S. Zang: *Metall. Mater. Trans. A*, 2006, vol. 37A, pp. 2459–69.
35. B. Zhou, Y.-L. Li, L.-Q. Xing, C.-S. Chen, H.-C. Kou, and J.-S. Li: *Philos. Mag. Lett.*, 2007, vol. 87, pp. 595–601.
36. K. Lee, S.-B. Lee, S.-K. Lee, and S.H. Lee: *Metall. Mater. Trans. A*, 2008, vol. 39A, pp. 1319–26.
37. M.L. Wang, X. Hui, and G.L. Chen: *J. Mater. Res.*, 2008, vol. 23, pp. 320–27.
38. H.F. Zhang, H. Li, A.M. Wang, H.M. Fu, B.Z. Ding, and Z.Q. Hu: *Intermetallics*, 2009, vol. 17, pp. 1070–77.
39. K. Lee, C.-Y. Son, S.-B. Lee, S.-K. Lee, and S.H. Lee: *Mater. Sci. Eng. A*, 2010, vol. 527, pp. 941–46.
40. C.-Y. Son, G.S. Kim, S.-B. Lee, S.-K. Lee, H.S. Kim, H. Hun, and S.H. Lee: *Metall. Mater. Trans. A*, 2012, vol. 43A, pp. 4088–96.
41. G. Rong, D.W. Huang, and M.C. Yang: *Theor. Appl. Fract. Mech.*, 2012, vol. 58, pp. 21–27.
42. B. Zhang, H.M. Fu, P.F. Sha, Z.W. Zhu, C. Dong, H.F. Zhang, and Z.Q. Hu: *Mater. Sci. Eng. A*, 2013, vol. 566, pp. 16–21.
43. H. Zhang, L.Z. Liu, Z.F. Zhang, K.Q. Qiu, X.F. Pan, H.F. Zhang, and Z.G. Wang: *J. Mater. Res.*, 2006, vol. 21, pp. 1375–84.
44. C.M. Warwick and T.W. Clyne: *J. Mater. Sci.*, 1991, vol. 26, pp. 3817–27.
45. F.P. Beer, E.R. Johnston, Jr., and J.T. Dewolf: *Mechanics of Materials*, 3rd ed., McGraw-Hill, New York, NY, 2002.
46. H.A. Bruck, T. Christman, A.J. Rosakis, and W.L. Johnson: *Scripta Metall.*, 1994, vol. 30, pp. 429–34.
47. L.F. Liu, L.H. Dai, Y.L. Bai, B.C. Wei, and J. Eckert: *Mater. Chem. Phys.*, 2005, vol. 93, pp. 174–77.
48. M.Q. Jiang, Z. Ling, J.X. Meng, and L.H. Dai: *Philos. Mag.*, 2008, vol. 88, pp. 407–26.
49. R.D. Conner, W.L. Johnson, N.E. Paton, and W.D. Nix: *J. Appl. Phys.*, 2003, vol. 94, pp. 904–11.
50. Y. Chen, M.Q. Jiang, and L.H. Dai: *Int. J. Plast.*, 2013, vol. 50, pp. 18–36.
51. Z.Y. Liu, L.S. Cui, Y.N. Liu, D.Q. Jiang, J. Jiang, X.B. Shi, Y. Shao, and Y.J. Zheng: *Scripta Mater.*, 2014, vol. 77, pp. 75–78.
52. D.E. Grady: *J. Mech. Phys. Solids*, 1992, vol. 40, pp. 1197–1215.
53. D.E. Grady: *Mech. Mater.*, 1994, vol. 17, pp. 289–93.
54. M.Q. Jiang and L.H. Dai: *Acta Mater.*, 2011, vol. 59, pp. 4525–37.
55. C.-Y. Son, G.S. Kim, S.-B. Lee, S.K. Lee, H.S. Kim, and S.H. Lee: *Metall. Mater. Trans. A*, 2012, vol. 43A, pp. 1911–20.
56. L. Varga, L. Bartha, A.J. Nagy, V. Stefaniay, and B. Borossary: in *Proc. Fifth Confer. Dimensioning and Strength Calculations, 6th Confer. Mater. Test.*, vol. 1, Akademiai Kiado, Budapest, 1974.
57. X.Q. Lei, Y.J. Wei, Z. Hu, and W.H. Wang: *Philos. Mag. Lett.*, 2013, vol. 93, pp. 221–30.